A comparison of shot-encoding schemes for wave-equation migration

Jeff Godwin & and Paul Sava
Center for Wave Phenomena, Colorado School of Mines

ABSTRACT
In the last decade the seismic imaging industry has begun collecting data volumes with a substantial amount of data redundancy through new acquisition geometries including: wide-azimuth, rich-azimuth and full-azimuth geometries. The increased redundancy significantly improves image quality in areas with complex geology, but requires considerably greater computational power to construct an image because of the additional data and the need to use advanced imaging algorithms. One way to reduce the computational cost of processing such datasets is to blend shot-records, using shot-encoding, together prior to imaging which reduces the number of migrations necessary for imaging. The downside to doing so is that blending introduces strong, non-physical, cross-talk noise into the final image. By carefully choosing the shot-encoding scheme, we can reduce the additional noise inserted into the image and maximally reduce the number of migrations necessary. To find an optimal encoding scheme, we develop a theory of blended imaging that describes all shot-encoding schemes, and design a new class of encodings that use amplitude weights instead of phase-shifts or time-delays. We are able to use amplitude encoding to produce blended images of the same quality as previous encoding schemes at a similiar computational cost. Additionally, we compare the results of amplitude encoding with the results from well-known shot-encoding schemes from previous work including decimated shot-record migration. In our comparison, we find that no single shot-encoding scheme is always better than others, and that decimated shot-record migration has some advantages over blended imaging. Overall, this work questions the potential for shot-encoding in standard seismic imaging workflows because blended imaging does not appear to justify its use by sufficiently reducing the cost of imaging, given the quality of the blended image.

Key words: imaging, wave-equation, simultaneous source, blended

1 INTRODUCTION

Today's seismic exploration challenges include imaging areas with complex geology, such as salt domes and overthrust regions. The major issues for imaging areas with complex geology are poor data quality and lack of seismic illumination due to the severe deformation of the seismic wavefield. One approach to resolve these issues is to obtain large amounts of redundant information from various acquisition directions via wide-azimuth or full-azimuth seismic surveys (Michell et al., 2006; Shoshitaishvili et al., 2006; Howard, 2007; Kapoor et al., 2007; Ting and Zhao, 2009). However, wide-azimuth surveys require significantly more time to acquire and even greater amounts of time to process due to the large amounts of data. Subsequently, the cost of acquiring and processing a wide-azimuth survey is significantly more expensive than the cost of a conventional survey. Additionally, the cost of imaging in complex geology is much greater because advanced imaging algorithms such as reverse-time migration must be used to better honor the kinematics of complex wavefields. Therefore, both the financial and computational cost of today's large surveys is increasing at a rapid pace, but recent technological advances may allow us to reduce these costs by using better processing technologies and faster computers for imaging.

One such technology is acquisition using simultaneous or delayed sources (Womack, 1990; Hampson et al., 2008; Berkhout et al., 2008; Beasley, 2008; Blacquiere et al., 2009). As the name implies, simultaneous sources are triggered at the

same time but at different spatial locations. By acquiring multiple sources in a shot-gather, a full-survey may be acquired in much less time than what is currently required. The downside to simultaneous source acquisition is that it creates additional noise in the final seismic image. Past research has circumvented the additional noise by de-blending the simultaneous source shot-gathers to create separate shot-gathers, as would be collected in a conventional survey, for each source prior to imaging (Spitz et al., 2008; Moore et al., 2008; Hampson et al., 2008; Akerberg et al., 2008; Kim et al., 2009; Huo et al., 2009). The separated shot-gathers are imaged using conventional shot-record migration (SRM) to produce the final image. The drawback to separating the shots is two-fold:

- First, the sources must be separable, which typically implies that they are relatively isolated from one another in space. This constraint limits the maximum amount of shots that can be used at once during acquisition.
- Second, the imaging process is not sped up by separating the shots because each separated shot must be imaged separately, as in SRM.

Because of these and other issues (e.g. logistical constraints associated with having multiple sources at once), industry has been reluctant to acquire datasets with many simultaneous sources at once.

A related idea, that aims to reduce the cost of imaging large datasets is to use multiple sources at once during imaging, which emulates simultaneous source acquisition. This process, known as blended imaging, combines multiple shot-gathers together prior to migration, which reduces the number of migrations that are needed to produce a final image (Morton, 1999; Liu, 1999; Romero et al., 2000; Soubaras, 2006; Zhang et al., 2007; Perrone and Sava, 2009; Berkhout et al., 2009). Certain forms of blended imaging, most notably plane-wave migration, are used in industry today, but many forms of blending (e.g. random phase) are not used today because they introduce a significant amount of noise to the image. However, the presence of the noise may be justified if the cost advantage over conventional shot-record migration is sufficiently high.

In order to illustrate how blending affects the cost of imaging, we first examine the cost of conventional shot-record migration. In shot-record migration, seismic data corresponding to individual shots are backpropagated independently to reconstruct the corresponding receiver-wavefield. Concurrently, the source-wavefield for each shot is constructed by forward propagating the source using a known velocity model. An imaging condition is then applied to the individual reconstructed source and receiver wavefields to produce an image of the subsurface. Because this process is repeated for each shot, the cost of shot-record migration (SRM) may be expressed as

$$C_{SRM} = N_s C_s, \tag{1}$$

where C_{SRM} is the total cost in computation time, N_s is the number of shot records, and C_s is the computational cost for imaging each shot. Since modern seismic surveys often consist of many tens of thousands of shots, and each shot may image a large area (a few km^2), the overall computational cost for imaging a seismic survey is tremendous.

However, equation 1 hints at a few possibilities to reduce the overall cost of imaging:

- reduce the cost of migrating each shot (i.e. reduce C_s), while keeping N_s constant, or
- reduce the number of shot-records used for migration (i.e. reduce N_s), while keeping C_s constant, or
- reduce both the cost of migrating each shot, C_s, and reduce the number of migrations necessary, N_s, at the same time.

In most scenarios, reducing the cost of migrating each shot C_s is the most practical approach to reducing the cost of imaging because one can choose the algorithm that is used for wavefield reconstruction (e.g. downward continuation or reverse-time migration). However, much of today's imaging is done in areas with complex geology, so computationally expensive algorithms like reverse-time migration have to be used to produce accurate images. Therefore, most reductions in computational cost, C_s, typically come from advances in computer hardware. In most cases however, our ability to create more demanding algorithms, for example: full anisotropic reverse-time migration, and acquire more data greatly exceed the rate of hardware advances (Zhang et al., 2005).

Furthermore, reducing the number of shots (i.e. decimating the dataset), N_s, that are used during imaging is not typically an option because both the signal-to-noise ratio and the illumination of the seismic image are negatively impacted by removing sources. An alternative to directly reducing the number of sources is to linearly combine multiple, independent shot-records together into blended shot-records prior to migration (Romero et al., 2000). By doing so, we effectively reduce the number of migrations that are necessary from N_s to N_e, where N_e is the number of blended shot-gathers or experiments. Therefore, the total cost of imaging using a blended migration scheme becomes:

$$C_{BRM} = N_e C_e. \tag{2}$$

In equation 2, C_{BRM} is the total cost for a blended source migration, C_e is the cost of an individual blended record migration, which we assume to be the same as the SRM cost C_s. In practice, $C_e > C_s$ as blended shots must be migrated over a larger migration aperture as in plane-wave migration (Romero et al., 2000). In general, as the number of blended experiments, N_e, decreases the overall cost of blended imaging decreases. In most instances, the reduction in cost by blending greatly outweighs the additional cost of extending the migration aperture as $N_e \ll N_s$, whereas C_e is only *somewhat* greater than C_s. The ultimate goal of blended imaging is to image using all shots in a single migration ($N_e = 1$), but a more realistic goal for blended imaging may be to reduce the computational cost of imaging by at least an order of magnitude.

During the blending process, each shot-record is individually weighted (or phase-shifted) and then all the weighted shot-gathers are summed together to form a blended shot-gather prior to migration (Morton, 1999; Liu, 1999; Romero et al., 2000; Soubaras, 2006; Zhang et al., 2007; Perrone and Sava, 2009; Berkhout et al., 2009). To form a shot-encoding scheme, a series of blended shot-gathers are produced by

changing the weights for each shot-record from one blended experiment to another. The way that the weights are changed from experiment to experiment, determines the type of encoding, and the characteristics of that encoding scheme (Liu, 1999; Romero et al., 2000; Perrone and Sava, 2009). After the shot-records are encoded, the source- and receiver-wavefields are reconstructed for the blended experiments exactly as in conventional shot-record migration. To produce an image using the blended wavefields we can apply the conventional cross-correlation imaging condition to the reconstructed wavefields as follows,

$$R_e(\mathbf{x}) = \sum_e \sum_t \left(\sum_i A_e^i W_s^i(\mathbf{x},t) \right) \left(\sum_j A_e^j W_r^j(\mathbf{x},t) \right), \qquad (3)$$

where i and j are the shot-record indices, $W_s^i(\mathbf{x},t)$ is the i^{th} reconstructed source wavefield, $W_r^j(\mathbf{x},t)$ is the j^{th} reconstructed receiver wavefield, e represents the blended shot-gathers index, A_e^i or A_e^j represents the shot-encoding weight for i^{th} or j^{th} shot-record for the e^{th} blended experiment, t represents time, $\mathbf{x}$ is a vector of locations in space. When $i = j$, equation 3 computes the correlation of wavefields related to a single shot gather. Conversely, when $i \neq j$, equation 3 computes the image for wavefields that are not physically related to one another, which introduces strong, coherent noise into the image that is indistinguishable from the desired image. This strong noise is referred to as crosstalk (Romero et al., 2000). As equation 3 shows, the crosstalk terms exist for each blended experiment for each source and every other receiver wavefield which means that there is a significant amount of crosstalk in the final image. Due to the negative impact of crosstalk noise on final image quality, crosstalk noise must be sufficiently attenuated during the imaging procedure. Previous attempts to remove the crosstalk terms in equation 3 have focused on phase-shifting the shot-records to shift the wavefields out of phase with one another. This methodology was first proposed by Rietveld (1994) who used phase-shifts to create wavefields with optimal illumination in complex geology. The prospect of imaging with blended wavefields was then more-or-less neglected until Tieman (1997) (re)introduced plane-wave migration, and Morton (1999) used random phase-shifts to speed up imaging. Some of the more prominent phase-encoding schemes include: plane-wave (Temme, 1984; Tieman, 1997; Stork, 1999; Liu, 1999; Duquet, 1999; Stoffa et al., 2006; Zhang et al., 2005; Liu et al., 2006; Shan and Biondi, 2008), random (Romero et al., 2000), harmonic (Zhang et al., 2007), plane-wave with dithering (Perrone and Sava, 2009), and frequency dependent, sign-opposite (Sun, 1999). It is important to note that many of these schemes choose to use linear phase-shifts as a function of frequency, and are therefore time-delay encodings. Of these encoding schemes, plane-wave is the most widely used. A recently developed encoding scheme is to use frequency independent phase-shifts in a modulated migration scheme (Soubaras, 2006).

Regardless of the shot-encoding scheme chosen, the most powerful method for attenuating crosstalk noise is to simply stack the images over many blended experiments (or realizations) that have different crosstalk characteristics because the

[htbp]

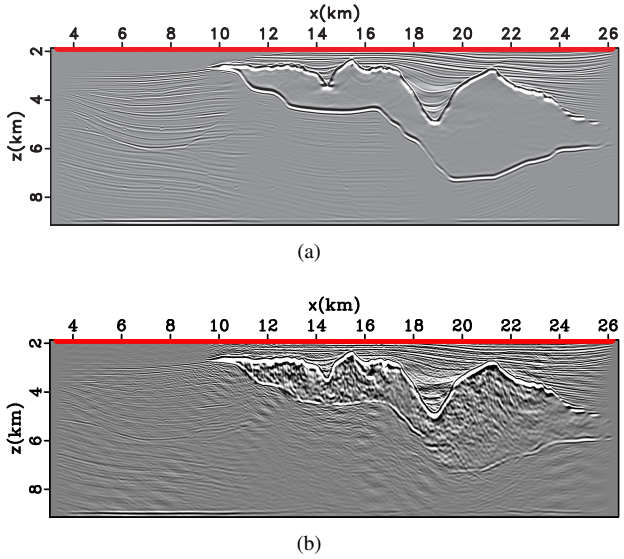


Figure 1. An example of how crosstalk contaminates the final stacked image for blended images. The (a) image obtained by conventional shot-record migration, (b) is the image obtained by random time-delay encoding, which introduces crosstalk artifacts that severely degrade the quality of the image.

desired image stacks together, while the incoherent crosstalk noise stacks out (Romero et al., 2000). However, simple stacking is not sufficient to completely remove most of the crosstalk for many shot-encoding schemes at a suitable cost advantage over shot-record migration because crosstalk noise is not completely incoherent from one blended experiment to another (i.e. crosstalk noise stacks together) (Romero et al., 2000). Thus, it is crucial to select encoding schemes that minimize the crosstalk noise during the imaging process. Subsequently, the two most important unresolved questions regarding blended imaging are: Does an optimal shot-encoding scheme exist that produces the best possible image at the lowest possible computational cost? If not, which of the already known shot-encoding schemes should be used?

The main goal of our work is to identify new shot-encoding schemes and to compare them against previously known shot-encoding schemes. By doing so, we aim to demonstrate which shot-encoding schemes produce the best quality image at the lowest possible cost. To design new encoding schemes, we develop a theory of blended imaging that reframes the process of blending in terms of matrix operations, Section 2. Using the theory that we outline, we are able to develop amplitude encoding schemes in Section 3, which do not require phase-shifts or time-delays for blending, a potential advantage in time-domain imaging. In Section 4, we demonstrate how the same theory explains previously known shot-encoding schemes, including: plane-wave migration, modulated-shot migration and random time-delay encoding. Additionally, we compare the previously mentioned shot-encoding schemes against decimated shot-record migra-

tion which is a possible alternative to shot-encoding. Lastly, we perform a theoretical cost analysis for blended imaging and decimated shot-record migration which shows that the purported cost advantage of blending may be much less than previously stated. Overall, we find that an optimal shot-encoding scheme may not exist.

2 THEORY

As previously noted by Tieman (1997) and Soubaras (2006) conventional seismic imaging can be described by a series of matrix operations, which can be expanded to include blended source imaging. Additionlly, the matrix representation allows us to determine the overall suitability of a shot-encoding scheme by determining the amount of crosstalk in the migrated image in advance.

To start, we revisit conventional shot-record migration, which is composed of two steps: wavefield reconstruction and the application of an imaging condition, which produces an image R as follows,

$$R(\mathbf{x}) = \sum_t \sum_i W_s^i(\mathbf{x},t) W_r^i(\mathbf{x},t). \tag{4}$$

For each shot gather, the source- and receiver-wavefields, W_s^i and W_r^i respectively, are reconstructed separately. Then, the two wavefields are cross-correlated and summed over time or frequency, depending on the domain, to form a partial image. All of the partial images are then stacked together to form the final image. Mathematically, each source and receiver-wavefield can be thought to be an element in a vector that holds all source- or receiver-wavefields respectively,

$$\mathbf{W}_S = \left[W_S^1, W_S^2, ..., W_S^i, ..., W_S^{N_s}\right], \tag{5}$$

$$\mathbf{W}_R = \left[W_R^1, W_R^2, ..., W_R^i, ..., W_R^{N_s}\right], \tag{6}$$

where $\mathbf{W}_S$ and $\mathbf{W}_R$ are row vectors, N_s is the number of shot-gathers, composed of the reconstructed wavefields, W_S^i and W_R^i, respectively. The i^{th} elements of both $\mathbf{W}_S$ and $\mathbf{W}_R$ correspond to the same physical shot-gather. Thus, conventional seismic imaging is equivalent to the inner product of the two vectors,

$$R = \mathbf{W}_S \mathbf{W}_R^H, \tag{7}$$

where R is the constructed image, H is the complex-conjugate transpose, and the multiplication of two elements of the matrix is actually the application of the imaging condition between those wavefields. As indicated earlier, the application of the imaging condition implies a summation over either time or frequency depending on which domain we use for wavefield reconstruction. The summation over elements of the vectors implies stacking the partial images together.

2. 1 The encoding matrix

In order to expand this notation to blended source imaging, we make use of the encoding matrix $\mathbf{E}$ (Tieman, 1997; Soubaras, 2006). The encoding matrix is $N_s \times N_e$, where N_e is the number of blended experiments and N_s is the number of shots (wavefields) in the survey. Each column in the encoding matrix corresponds to a single blended experiment (realization), while each row acts as a weight for a particular source- or receiver-wavefield. Thus, each column in the encoding matrix weighs all wavefields to determine how to combine them together prior to imaging. To formally define the encoding matrix, we introduce the notation $E_{m,n}$, where the m index corresponds to the row (or shot index) and n corresponds to the colum, or blended experiment index. The encoding matrix contains weights which may be fractional, positive or negative, and may even be complex-valued. We note that the physical meaning of the weights changes based on their format. For example, real-valued weights correspond to weighting the entire contribution of full wavefields (amplitude encoding), whereas complex-valued weights represent phase-shifting. Additionally, it is possible to combine both amplitude and phase-shifts together, which can be represented mathematically as,

$$\mathbf{E}_{m,n} = A_{m,n} \exp(-j\phi_{m,n}), \tag{8}$$

where A is the amplitude weight for the m^{th} shot-record for the n^{th} blended experiment, $\phi_{m,n}$ is the corresponding phase-shift for that shot-record, and j is the $\sqrt{-1}$. Amplitude only encodings are represented in equation 8 by letting $\phi_{m,n} = 0$ for all m and n. Conversely, phase-encodings are obtained when $A_{m,n} = 1$ for all m and n.

Because we generally assume that we can treat frequencies independently from one another, a different encoding matrix may exist for each frequency simultaneously. Thus, the encoding matrix is actually a three-dimensional matrix whose third dimension is frequency, ω, and $\mathbf{E}$ is a function of ω in the most general case (Soubaras, 2006). Mathematically, we represent the frequency-dependence of an element in the encoding matrix as:

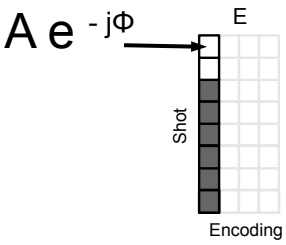
$$\mathbf{E}_{m,n}(\omega) = A_{m,n}(\omega) \exp(-j\phi_{m,n}(\omega)) \tag{9}$$

where $A_{m,n}(\omega)$ is the amplitude weight for the frequency, ω, and $\phi_{m,n}(\omega)$ is the phase-shift for the same frequency. A special case of frequency dependent phase-encodings are time-delay encodings where $\phi_{m,n}(\omega) = 2\pi\omega\tau_{m,n}$, which causes a linear-shift of phase as a function of frequency. Due to the symmetry of the time and frequency domain, it is also possible to consider time-dependent encodings, where a different encoding is used for each time-step, but it is not clear if there is an advantage to doing so.

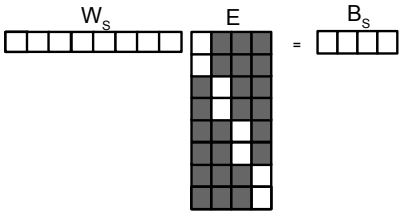
For simplicity we only consider the frequency independent case where $\mathbf{E}(\omega) = \mathbf{E}$ for all ω, but the framework that we develop is equally valid for both frequency dependent and frequency independent encodings. For reference, Figure 2(b) depicts a sample amplitude-only encoding matrix where the weights are real-valued, binary (1 or 0) whose effect is to select only some wavefields per blended experiment.

2. 2 Matrix representation of blended imaging

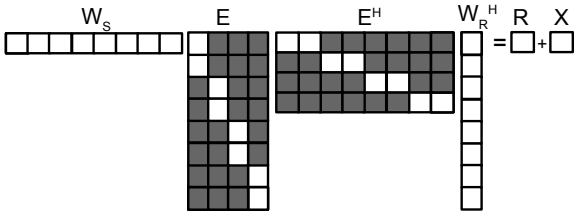
The encoding matrix reduces the effective number of reconstructed wavefields that are used for imaging by projecting the



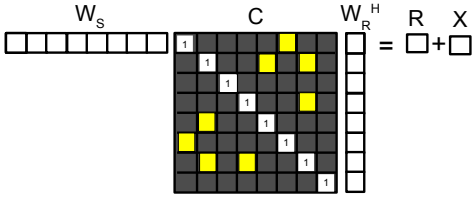
(a)



(b)



(c)



(d)

Figure 2. The encoding matrix (a) is composed of weights of the form $A\exp(-j\phi)$ where A is the amplitude weighting term, and ϕ is the phase-shift to be applied. To blend the wavefields, we project the wavefield vector onto the encoding matrix (b) to produced the blended wavefield vector $\mathbf{B}_S$. By performing the necessary substitutions, the entire blended imaging process (c) can be summed up as the product of matrix multiplications. The crosstalk matrix (d) is the product of the encoding matrix with its transpose.

wavefield vector onto the encoding matrix, thereby reducing the dimensionality of the wavefield vector as follows:

$$\mathbf{B} = \mathbf{WE}, then \begin{cases} \mathbf{B}_S &= \mathbf{W}_S\mathbf{E} \\ \mathbf{B}_R &= \mathbf{W}_R\mathbf{E} \end{cases} \tag{10}$$

where $\mathbf{WE}$ is the projection of the wavefield vector (i.e. $\mathbf{W}_S$ or $\mathbf{W}_R$) onto the encoding matrix $\mathbf{E}$, and $\mathbf{B}$ is the blended wavefield vector for the source- or receiver-wavefields (i.e. $\mathbf{B}_S$ or $\mathbf{B}_R$). Therefore, $\mathbf{B}_S$ is the $1 \times N_e$ row vector of combined source-wavefields and $\mathbf{B}_R$ is an $N_e \times 1$ column vector of combined receiver-wavefields. Because the migration operator is linear, we can perform the combination of the source- and receiver-data, the product of $\mathbf{WE}$, prior to wavefield reconstruction, thus reducing the necessary number of migrations from N_s to N_e. The final blended source image R_e is represented by

$$R_e = \mathbf{B}_S\mathbf{B}_R^H, \tag{11}$$

and is shown in 2(c) . By substituting the expressions for $\mathbf{B}_S$ and $\mathbf{B}_R$ from equation 10 into equation 11, we obtain

$$R_e = \mathbf{W}_S\mathbf{E}\mathbf{E}^H\mathbf{W}_R^H, \tag{12}$$

which is similar to equation 7 and shown in Figure 2(c). We refer to the product $\mathbf{EE}^H$ as the crosstalk matrix $\mathbf{C}$, which is square and has dimensions of $N_s \times N_s$, Figure 2(d). Thus, equation 12 can be written as

$$R_e = R + X = \mathbf{W}_S\mathbf{C}\mathbf{W}_R^H, \tag{13}$$

where X represents the crosstalk noise added to the conventional image. The crosstalk matrix $\mathbf{C}$ is similar to the identity $\mathbf{I}$, but with additional off-diagonal terms as shown in 2(d). This is a convenient description because equation 7 can be rewritten to include the identity matrix $\mathbf{I}$ to represent the pairing of each source wavefield with its corresponding receiver wavefield as:

$$R_e = R = \mathbf{W}_S\mathbf{I}\mathbf{W}_R^H. \tag{14}$$

Thus, the $\mathbf{C}$ matrix represents the formation of the conventional seismic image (i.e the diagonal terms) plus additional terms in the off-diagonals representing the pairing of wavefields that are not physically related to one another. Subsequently, the off-diagonal components of the $\mathbf{C}$ matrix are the crosstalk terms that we generate by using a certain encoding matrix $\mathbf{E}$ (Tieman, 1997; Soubaras, 2006).

2. 3 Designing optimal shot-encoding schemes

By examining equations 13 and 14, we find that optimal shot-encoding schemes should have a crosstalk matrix $\mathbf{C}$ that is as close to the identity matrix $\mathbf{I}$ as possible in order to minimize the crosstalk in the image R_e, (Tieman, 1997; Soubaras, 2006). Consequently, the process of choosing a shot-encoding scheme becomes one of finding an encoding matrix $\mathbf{E}$ such that $\mathbf{EE}^H$ has the fewest off-diagonal components, or $\mathbf{EE}^H \approx \mathbf{I}$. If an encoding exists such that $\mathbf{EE}^H = \mathbf{I}$, then we can produce the same image as shot-record migration, at a cost proportional to the number of blended source experiments N_e, instead of N_s (Soubaras, 2006).

One possible set of encoding matrices are orthonormal bases. For reference, a matrix $\mathbf{Q}$ is defined to be an orthonormal basis if $\mathbf{Q}^H\mathbf{Q} = \mathbf{I}$ and $\mathbf{Q}\mathbf{Q}^H = \mathbf{I}$, which implies that the row and column vectors are orthogonal to one another, and that the norm of each vector is one. Thus, we reconstruct the identity matrix $\mathbf{I}$ from $\mathbf{E}\mathbf{E}^H$, if we use an orthonormal basis for our encoding matrix $\mathbf{E}$. Unfortunately, orthonormal bases are represented by square matrices of the same size as that of the parent matrix or the same size as $\mathbf{C}$ which is $N_s \times N_s$ in our case. Therefore, an orthonormal basis encoding matrix provides no cost advantage compared to standard shot-record imaging because we would have to perform N_s migrations, the same number as conventional shot-record migration. While it may not be possible to directly use an orthonormal basis for an encoding matrix, we can truncate the columns of the orthonormal basis to form an encoding matrix that provides a substantial cost reduction. The missing columns contain features from the image that are lost in the reconstructed image. This conclusion is similar to that obtained by Soubaras (2006) for the discrete Fourier basis. Other encoding schemes also use truncated orthogonal bases for the encoding matrix, even if it may not appear so at first glance. However, not all encoding schemes use a truncated orthogonal basis for the encoding matrix. For example, random time-delay encoding uses a pseudo-orthogonal encoding matrix (Romero et al., 2000). The advantage to using a pseudo-orthogonal encoding matrix is that the crosstalk is less coherent from one blended experiment to another, which generally improves image quality. The downside to using pseudo-orthogonal encodings is that there is no guarantee that we ever produce an image that matches the quality of conventional SRM.

2. 4 Cost comparison

One of the most important aspects of blended imaging is assessing the computational advantage that blending provides relative to conventional shot-record migration and to other encodings. To do so, we compare the cost of conventional shot-record migration, equation 1, with the cost of blended imaging, equation 2. However it's not clear whether there is a real cost-advantage to blended imaging merely be examining equation 1 and equation 2 because C_e is usually greater than C_s due to the larger migration volume, while N_e is less than N_s due to blending. To gain more insight, we expand C_e and C_s for the case of downward continuation migration in three dimensions. For downward continuation, the cost of migrating a single shot-record is proportional to:

$$C_s = 2FN_xN_yN_zN_\omega = 2FL_sN_\omega \tag{15}$$

In equation 15, N_x, N_y and N_z are the number of points in the migration volume for a single shot-record in their respective dimensions, N_ω is the number of frequencies, F is the number of floating point operations per point in space and frequency, and 2 represents the cost of extrapolating both the source and receiver wavefields. We combine $N_xN_yN_z$ into a single term L_S, which is the migration volume for a single shot-record. In the blended case, the migration volume L_e is the number of distinct points from the migration volume of each shot-gather in the blended shot-gather. For example, if the blended shot-record consists of shot-records that have independent migration volumes (i.e. the volumes do not overlap), then $L_e = N_sL_s$. Conversely, if the blended shot-gather is composed of shots that have almost identical migration volumes (i.e. the volumes overlap), then L_e is the number of distinct points in sum of the individual shot-record migration volume. Mathematically, L_e is described as the distinct union of all points in the migration volumes for all shot-gathers in the blended shot gathers as follows:

$$L_e = L_s^1 \cup L_s^2 \cup L_s^3 ... L_s^N. \tag{16}$$

By substituting equation 16 into equation 15, we produce the following expression for the cost of migrating a single blended shot-gather,

$$C_e = 2FL_eN_\omega. \tag{17}$$

We take the ratio of equation 1 and equation 2, substituting the appropriate values for C_s and C_e to produce,

$$\Gamma = \frac{2FL_SN_SN_\omega}{2FL_BN_BN_\omega} = \frac{L_SN_S}{L_BN_B} \tag{18}$$

where Γ is the cost ratio of shot-record migration to blended record migration. The value of Γ directly gives us a relative cost-ratio of shot-record migration to blended migration. For example, if Γ is greater than one, then blended imaging is more efficient than shot-record migration. Conversely, if Γ is less than one, then shot-record migration is more efficient than blended imaging. For practical purposes, a blended imaging scheme must at least be more efficient than break-even with SRM ($\Gamma \geq 1$) to be considered a success, while a good blending scheme would significantly reduce the cost of imaging by at least two-fold, $\Gamma > 2$. It is important to note that the reduction in the number of experiments needed for blended imaging N_e is countered by the increase in the migration volume L_e (Liu, 1999; Romero et al., 2000; Zhang et al., 2005).

If the encoding matrix is frequency dependent, then the cost of blended imaging may depend on frequency if the number of encodings varies as a function of frequency. Thus, equation 2 becomes:

$$C_{BRM} = 2FL_e\sum_\omega N_e(\omega). \tag{19}$$

Again, taking the ratio of equation 19 and equation 1, we arrive at the following expression in the most general of terms for the ratio of the cost of blending and shot-record migration:

$$\Gamma = \frac{L_sN_sN_\omega}{L_e\sum_\omega N_e(\omega)}. \tag{20}$$

As with equation 18, when the value of Γ in equation 20 is less than 1, then SRM is less costly than blended imaging. If Γ is greater than 1, then SRM is more costly than blended imaging.

3 AMPLITUDE ENCODING

We demonstrate how the theory that we have developed can be used to construct a new class of encodings that we refer to as

amplitud encodings. Amplitude encodings are shot-encodings that weight the whole wavefield for each shot at once. The advantage to using amplitude encodings is that we do not have to use phase-shifts or time-delays. One amplitude encoding that we have developed is the Hartley encoding.

3. 1 Hartley basis

A well-known orthonormal basis is the complex-valued discrete Fourier matrix (Strang, 1997; Oppenheim, 1999; Soubaras, 2006). A real-valued alternative to the Fourier basis is the Hartley basis (Strang, 1997; Tsitsas, 2010). The Hartley encoding matrix is defined as,

$$\mathbf{E}_{m,n} = cos\left(\frac{2\pi mn}{\wp}\right) + sin\left(\frac{2\pi mn}{\wp}\right), \tag{21}$$

where m is the shot-index, n is the encoding index, and $\wp$ is the periodization index (Soubaras, 2006). The relation to the Fourier transform is directly apparent, but the presence of the addition between the sine and cosine introduces additional cross-terms into the crosstalk matrix as follows,

$$\begin{aligned}\mathbf{C}_{k,l} = \sum_{n=0}^{N_e} & cos(\psi_k)cos(\psi_l) + cos(\psi_k)sin(\psi_l) \\ & + sin(\psi_k)cos(\psi_l) + sin(\psi_k)sin(\psi_l),\end{aligned} \tag{22}$$

where $\psi_k = 2\pi kn/\wp$ and $\psi_l = 2\pi ln/\wp$. From equation 22 it is clear that there are additional off-diagonal components represented by the cross-terms between the $cos(x)sin(y)$ terms present in the expression. We note, that the cross-terms may be removed by using negative frequency values for the same encodings in equation 21 and then adding them to equation 21, because the sine function is odd (e.g. $sin(-x) = -sin(x)$). However, doing so would double the number of encodings required, from N_e to $2N_e$, or more importantly half the number of encodings that we are able to use to capture unique information in the encoding matrix. Halving the number of encodings with unique information is detrimental to the image quality because each encoding captures additional spatial information in the image (Stork, 1999; Zhang et al., 2005; Soubaras, 2006).

To understand why this is the case, we consider the relationship between sinusoids and spatial sampling theory. This relationship is derived directly from the encoding matrix by converting equation 21 from shot-indices to spatial coordinates. For example, if we let $m = x_m/\Delta x$ where Δx is the shot-sampling interval, and x_m is the actual shot-location in space, then equation 21 becomes:

$$\mathbf{E}_{m,n} = cos\left(2\pi x_m n/(\Delta x\wp)\right) + sin\left(2\pi x_m n/(\Delta x\wp)\right). \tag{23}$$

Using the relationship between the spatial-wavenumber, K, and the spatial sampling interval, $\Delta K = 1/\wp\Delta x$, then equation 23 is equivalent to:

$$\mathbf{E}_{m,n} = cos\left(2\pi x_m n\Delta K\right) + sin\left(2\pi x_m n\Delta K\right). \tag{24}$$

From equation 23 it is clear that when the encoding matrix is square (i.e. $N_e = N_s$) then the encoding matrix is unitary because the complete sum of sinusoids is unitary. Additionally, equation 24 shows that each additional encoding (specified by the n-index) increases the angular frequency of the argument to the sine and cosine functions. By using the relationship, $K = n\Delta K$, equation 24 shows that each additional encoding adds another spatial wave-number to the encoding matrix up to the maximum spatial wave-number as specified by the Nyquist sampling criterion (i.e. in the limit the encoding is equivalent to SRM). However, when we truncate the Hartley basis or truncate the encoding matrix, we restrict the maximum sampled wave-number, which means that the image is not fully sampled in the wave-number domain. Since we usually prefer to keep encodings corresponding to low wave-numbers, we wind up constructing an encoding matrix that is equivalent to an ideal low-pass spatial filter that uses the Hartley transform.

As equation 23 shows, the periodization index, $\wp$, is also a critical parameter that greatly affects the outcome of a Fourier-related encoding scheme because if equation 21 is changed so that $\wp \neq N_s$, then the period of the sinusoids in the encoding matrix changes from N_s to $\wp$. By changing the period of the sinusoids we also change the spatial sampling rate, ΔK. Since ΔK is inversely proportional to the periodization distance, the spatial sampling interval increases when we reduce the periodization distance. This means that the same number of encodings obtain more spatial information and subsequently the quality of the image improves. At the same time, changing the periodization distance introduces strong, coherent crosstalk between shots that are now a full-period away from one another in the encoding matrix, because the weights for those shot-records are the same (i.e. shots that are $\wp$ away from one another have maximum crosstalk). However, this strong crosstalk, may be acceptable because there are situations in which some shots never contribute crosstalk to other shots. For example, consider the case where two shots are on opposite sides of a large survey. Those two shots likely have migration apertures that do not overlap, and thus are not likely to contribute crosstalk to the image even though cross-terms may exist between those shots in $\mathbf{C}$. For most surveys, the distance at which two shots do not share migration aperture is smaller than the total survey area, and so $x_\wp$ and subsequently $\wp$ may be much smaller than N_s depending on shot spacing. Formally this relationship is given as,

$$\wp_{min} = 2x_{aperture}/\Delta x, \tag{25}$$

where $x_{aperture}$ is the width in space of the migration aperture for one shot, assuming that all shots have the same migration aperture. As Soubaras (2006) notes, the minimum constraint for the periodization value, substantially affects the cost advantage of blended imaging, and so is a crucial parameter for Fourier-related blending schemes.

4 PHASE ENCODING

As Soubaras (2006) showed, the theory developed in Section 2 explains the results for a phase-shift encoding known as modulated-shot migration. We compare and contrast the efficiency of modulated-shot migration with the other shot-encoding schemes as well.

4. 1 Modulated-shot migration (DFT)

Modulated-shot migration, which we refer to as the DFT shot-encoding, is an encoding scheme that uses the discrete Fourier transform matrix as the encoding matrix (Soubaras, 2006). Formally, the encoding matrix is given as:

$$\mathbf{E}_{m,n} = \begin{cases} cos\,(Amn) - jsin\,(Amn)\,, & 0 \le n < N_e/2 \\ cos\,(Amn) + jsin\,(Amn)\,, & N_e \le n \le N_e \end{cases} \tag{26}$$

where m is the shot index, n is the encoding index, and A is $2\pi/\wp$ where $\wp$ is the periodization distance, which is typically N_s for the unitary DFT encoding matrix. Because we truncate the DFT matrix and we preferentially keep encodings corresponding to sinusoids with low angular frequencies, we can consider the DFT encoding matrix to be equivalent to an optimal low-pass filter. As with the Hartley encoding, we can consider the DFT encoding to operate in the wave-number domain as well by substituting the appropriate quantities $m = x_m/\Delta x$, which has implications for spatial sampling of the image. For example, modulated-shot migration only reconstructs the image up to a maximum wave-number, K_{max}, which is determined by the maximum angular frequency of the last encoding and is usually less than K_{nyq}. Additionally, equation 26 shows that modulated-shot migration must include both positive and negative values for K in order to properly illuminate the subsurface. We demonstrate the need for the positive and negative values of K by considering the case of a single encoding with a particular K value, whose encoding is represented as:

$$\mathbf{E}_k = exp(-jA\rho k) = cos(A\rho k) + jsin(A\rho k), \tag{27}$$

where A represents the collection of all terms (including K) in the numerator and denominator of equation 26 and k is the shot index. The crosstalk matrix for this single experiment is,

$$\mathbf{C}_{k,l} = \mathbf{E}\mathbf{E}^H = [cos(A\rho k) + jsin(A\rho k)][cos(A\rho l) - jsin(A\rho l)], \tag{28}$$

which further expands to,

$$\begin{aligned} \mathbf{C}_{k,l} =& cos(A\rho k)cos(A\rho l) \\ &+ jsin(\rho k)cos(A\rho l) \\ &- jsin(A\rho l)cos(A\rho k) \\ &+ sin(A\rho k)sin(A\rho l). \end{aligned} \tag{29}$$

The presence of the complex-valued terms in equation 29 represent phase-shifted crosstalk in the final image. We note that these terms vanish when $k = l$, which indicates that the desired image is not phase-shifted. In most cases, cross-terms from out of phase wavefields produce strong crosstalk that significantly degrades the quality of the image (Romero et al., 2000). However, the cross-terms in equation 29 have a regular pattern to them, which instead causes a distortion in the illumination of the final image. The simplest method to remove the cross-terms from equation 29 is to concatenate another encoding whose $A = -A$ because the sine function is odd. By substituting $A = -A$ into equation 29 we arrive at:

$$\begin{aligned} \mathbf{C}_{k,l} =& cos(A\rho k)cos(A\rho l) \\ &- jsin(A\rho k)cos(A\rho l) \\ &+ jsin(A\rho l)cos(A\rho k) \\ &+ sin(A\rho k)sin(A\rho l). \end{aligned} \tag{30}$$

Adding equation 29 and equation 30 eliminates the complex-valued terms from both expressions, and reduces both expressions to:

$$C_{k,l} = cos(A\rho k)cos(A\rho l) + sin(A\rho k)sin(A\rho l). \tag{31}$$

Thus, for every encoding in the DFT encoding matrix, we must include another encoding whose argument $A = -A$ for that particular encoding (Soubaras, 2006). This effectively doubles the number of encodings that must be used for the DFT encoding matrix which is the same requirement as that for the Hartley amplitude encoding. However, the penalty for not using these additional encodings is greater for the DFT encoding matrix because the illumination of the image is affected, whereas the additional cross-terms in the Hartley encoding produce additional crosstalk only.

It's interesting to note that the DFT and Hartley encoding can be made equivalent by using identical arguments for the cosine and sine functions in both encodings. When this is the case, then equation 22 equals equation 31, and the crosstalk matrix for modulated-shot migration (DFT encoding) is the same as the crosstalk matrix for the Hartley amplitude encoding. Physically, this means that the DFT and DCS encodings produce identical images. In this case, the only difference between the two encodings, is how they are physically implemented during the blending process (i.e. phase-shifts versus amplitude weights).

5 TIME-DELAY ENCODINGS

Additionally, we compare and contrast the results from two time-delay encoding schemes: plane-wave migration (Tieman, 1997; Liu, 1999; Zhang et al., 2005), and random time-delay encoding (Romero et al., 2000), with the other shot-encoding schemes.

5. 1 Plane-wave migration

For plane-wave migration, the encoding matrix is defined by the maximum time-delay and the number of encodings. As mentioned in the literature, the maximum time-delay also determines the maximum wave-number in the blended image, and subsequently the crosstalk present in the final image (Tieman, 1997; Duquet, 1999; Liu, 1999; Stork, 1999; Zhang et al., 2005). To illustrate this consider the expression for the frequency-dependent encoding matrix for plane-wave migration which is given by:

$$\mathbf{E}_{m,n}(\omega) = exp(-j\omega\tau_{m,n}), \tag{32}$$

where $\tau_{m,n}$ is the time-delay in seconds, at the m^{th} shot for the n^{th} plane-wave encoding. The time-delay, $\tau_{m,n}$, is related to

the shot position and the blended experiment by the relation,

$$\tau_{m,n} = \frac{(t_{max} - 2nt_{max}/N_e)m}{N_s} - \frac{t_{max} - 2nt_{max}/N_e}{2}, \quad (33)$$

where n is the n^{th} encoding, m is the shot index,Δx is the shot-sampling interval, t_{max} is the maximum time-delay in seconds, and N_e is the number of blended experiments. Equation 33 requires $2t_{max}$ because plane-wave migration must create plane-waves with both positive and negative time-delays to ensure proper illumination throughout the image. As Stork (1999) and Zhang et al. (2005) note, the take-off angle of the plane-wave is related to the spatial wave-number in the image. In order to reconstruct the highest wave-numbers in the image, we must use plane-waves with greater and greater take-off angles (time-delays). This is a major shortcoming to plane-wave migration in the time-domain because additional time-delays substantially increase the computational cost of reverse-time migration.

In any case, the crosstalk matrix for plane-wave migration is given by:

$$\mathbf{C}_{k,l}(\omega) = \sum_{n=0}^{N_e} exp(-j\omega[\tau_{k,n} - \tau_{l,n}]). \quad (34)$$

We expand equation 34 into:

$$\mathbf{C}_{k,l}(\omega) = \sum_{n=0}^{N_e} cos(\omega[\tau_{k,n} - \tau_{l,n}]) + jsin(\omega[\tau_{k,n} - \tau_{l,n}]). \quad (35)$$

We note that equation 35 is frequency dependent, meaning that a different crosstalk matrix exists for each frequency. In any case, when $k = l$ in equation 34, the complex-exponential is one, which produces the desired image. When $k \neq l$, then there is strong coherent crosstalk with a non-zero phase component (i.e. the sine term in equation 35 is non-zero). However, we note that when both positive and negative values of τ are swept, the sign of the phase-terms reverses, thereby removing them. Therefore, equation 35 is equivalent to the crosstalk matrices for both the Hartley and DFT encodings, equations 22 and 31 respectively, when the time-delays are sufficiently selected. However, the frequency-dependence of plane-wave migration is a significant difference between the encodings, which is why plane-wave migration and the other encodings do not produce the same result. As Stork (1999) shows, the time-delay for a given encoding can be converted to spatial wave-number. As with the DFT encoding, plane-wave migration requires two encodings for each spatial wave-number to properly illuminate the subsurface. It's important to note, that unlike the Hartley and DFT encodings, plane-wave migration evenly samples spatial wave-numbers up to a maximum wave-number that is determined by the maximum time-delay used.

5. 2 Random time-delay

Random time-delay encoding delays the shots using delays specified by a uniform distribution. The defining parameter for the uniform distribution is the maximum time-delay. Thus, the encoding matrix is given as:

$$\mathbf{E}_{m,n} = U(-t_{max}, t_{max}) \quad (36)$$

where U is a uniform probability distribution function with t_{max} the maximum time-delay for the shot-records. We can not formulate an analytic expression for the crosstalk matrix for random-time delay encoding. Instead, we can view the structure of the crosstalk matrix for one possible permutation of random time-delay encoding with the understanding that the crosstalk matrices for all similar encodings are more or less the same.

6 DECIMATED SHOT-RECORD MIGRATION

As Stork (1999) and others have noted blended imaging is comparable to decimating our shot-records prior to imaging. Therefore, it is important to understand how different shot-encoding schemes compare against decimated shot-record migration (DSRM), because decimated shot-record migration has a few significant advantages over blended imaging:

- DSRM is easier to implement than shot-encoding because it does not require blending prior to imaging, and
- DSRM is less computationally expensive than blended imaging because each shot-record is migrated over a smaller migration aperture.

There is one major downside to DSRM though: we know that by decimating our data we introduce spatial aliasing for reflectors with high wave-numbers. For example, if we change our shot-sampling interval from Δx to $10\Delta x$ (i.e. decimate our data by a factor of 10), then the maximum wave-number of a reflector that we can avoid aliasing in our image is now $1/10$ what it was before decimation due to the Nyquist criterion.

We note that it is also possible to consider DSRM as a shot-encoding scheme. To do so, we could construct an encoding matrix, whose columns consist of a single entry with all other rows being zero to select each individual shot-record for migration. Formally, the encoding matrix for DSRM is,

$$\mathbf{E}_{m,n} = \begin{cases} 1 & m = n\Delta s \\ 0 & \text{else,} \end{cases} \quad (37)$$

where Δs is the decimation factor (e.g. $\Delta s = 10$ to use every 10^{th} shot-record). The cross-talk matrix for decimated shot-record migration, is:

$$\mathbf{C}_{k,l} = \begin{cases} 1 & k = l = i\Delta s \\ 0 & \text{else.} \end{cases} \quad (38)$$

In equation 38, i represents integers in the range [0,1,...,$N_s/\Delta s$]. The cross-talk matrix for DSRM is simply a decimated identity matrix.

7 RESULTS

We compare the Hartley, DFT, Plane-wave, and random-time shot-encoding schemes for the original Sigsbee2A dataset, which is comprised of 500 shot-records. For each shot-encoding scheme, we construct the encoding matrix as previously discussed. For Hartley and DFT encodings we use a

periodization distance, $\wp = 250$, which is the optimal value for the Sigsbee dataset. For plane-wave and random-time delay encoding we use a maximum time-delay of 9.0 seconds, which is the theoretical maximum given by Stork (1999). After constructing the encoding matrix, we generate the crosstalk matrices, Figure 3, for each encoding for a number of encodings: 25, 50, 100, and 250. Additionally, we compare the results of the encodings against the results obtained by using decimated shot-record migration using the same number of shot-records as encodings. In this way, the number of migrations for blended imaging and decimated shot-record migration are identical. We migrate the blended or decimated data using split-step downward continuation. Figures 4-7, show the stacked images for all of the encoding schemes (including decimated SRM) and the difference images computed by subtracting the normalized blended image from the normalized image from conventional shot-record migration, Figure 1(a). To make the comparison of difference images easier, we amplify (approximately 20 $\times$) and clip the difference images from all shot-encodings to the same scale. This ensures that changes in the difference images from encoding to encoding are directly comparable. As the difference images show, Figures 4-7, the crosstalk from the different shot-encoding schemes manifests itself very differently in the final stacked images. In all cases the amount and strength of the crosstalk decreases as the number of encodings used increases. For decimated shot-record migration, the difference image shows the artifacts introduced by aliasing.

Additionally, we conduct a cost comparison of the various shot-encoding schemes as shown in Table 1. For each encoding we provide best-case and worst-case speed-up factors compared to shot-record migration. The best case scenario is simply the ratio of the number of encodings compared to the number of individual shots. In the worst case scenario, we include the effect of migrating over a larger migration aperture. In most cases, the actual speed-up relative to SRM is somewhere between these two values because the actual computational cost of imaging on modern computational hardware is more affected by hardware architecture and software optimization than our worst-case scenario depicts. The cost advantage of shot-encoding compared to decimated SRM is less than optimal.

We also compare the F-K spectra of the various shot-encoding schemes as Soubaras (2006) does. In this case, we consider the effect that encoding has on on the image in terms of which spatial wave-numbers are reconstructed in the image relative to all of the wave-numbers obtained using conventional shot-record migration. For example: Hartley, DFT and plane-wave encoding all reconstruct only certain wave-numbers in the image. Decimated shot-migration aliases high wave-numbers because we do not lowpass filter the shot-records before decimating. Figures 9(a)-9(d) show the wave-numbers that these encodings select for 50 encodings (or shot-records in the case of decimated SRM). In the F-K domain Hartley encoding has an advantage over DFT and plane-wave migration because they both spend encodings acquiring $-K$ values in order to ensure proper illumination of the image. Hartley encoding does not need to sample $-K$. Thus, Hartley amplitude encoding is able to reconstruct more of the spatial information in the image at the same computational cost of DFT and plane-wave migration. Plane-wave migration samples the F-K domain which introduces aliasing type artifacts in addition to crosstalk noise. However, because plane-wave migration reconstructs some of the highest wave-numbers as well, the images look much better than we would expect from just examining the F-K spectrum. By comparison, decimated SRM aliases the high wave-numbers in the image (black areas in Figure 9(d)), although these aliasing artifacts appear to be less coherent than crosstalk artifacts, Figures 4-7.

Lastly, we compare the shot-encodings on an absolute basis by ranking them relative to one another using a measure of the energy in the difference images, or quality of the image, for each encoding. Formally, the measure of energy is simply the l_2-norm of the difference image. As the energy in the difference image is minimized, the quality of the stacked image is maximized. Thus, the best shot-encoding at a given cost minimizes the value of the energy. Figure 8 shows the comparison of the various shot-encodings as a function of the number of encodings used by comparing the overall energy in the difference image. The results are quite striking, as some shot-encodings quickly approach zero in the difference image (i.e. image similar to that obtained by conventional SRM), while others such as: plane-wave migration have large differences regardless of the number of encodings used. Random-time delay encoding starts out with the smallest energy in the difference image, but then is quickly surpassed by other shot-encoding schemes.

8 DISCUSSION

Using a unified theory of blended imaging, we are able to design a new class of shot-encoding schemes that we refer to as amplitude encoding. For brevity, we only examine the Hartley encoding scheme that uses the real-valued Fourier transform matrix as the encoding matrix, but many other amplitude encoding schemes are possible such as random-polarity reversal (Krebs et al., 2009). The advantage to using amplitude encoding is that we can avoid using time-delays or phase-shifts for encoding. Hartley encoding has some advantages over similar phase-shift encodings (DFT) and plane-wave migration, in that Hartley encoding is able to recover more spatial information in the image than either the DFT encoding or plane-wave migration using the same number of encodings. Both Hartley and DFT encoding produce images that have reduced spatial information in the images because the encodings only capture low wave-number information during the blending process. As we add more encodings to both of these shot-encoding schemes we improve the spatial resolution of the image. We note that Hartley, DFT, and plane-wave migration all show amplitude distortion of the reflectors in the difference images, especially when fewer encodings are used (e.g. 25 and 50 encodings). The cause of this amplitude distortion is related to the interference of shots that are spatially close to one another in the

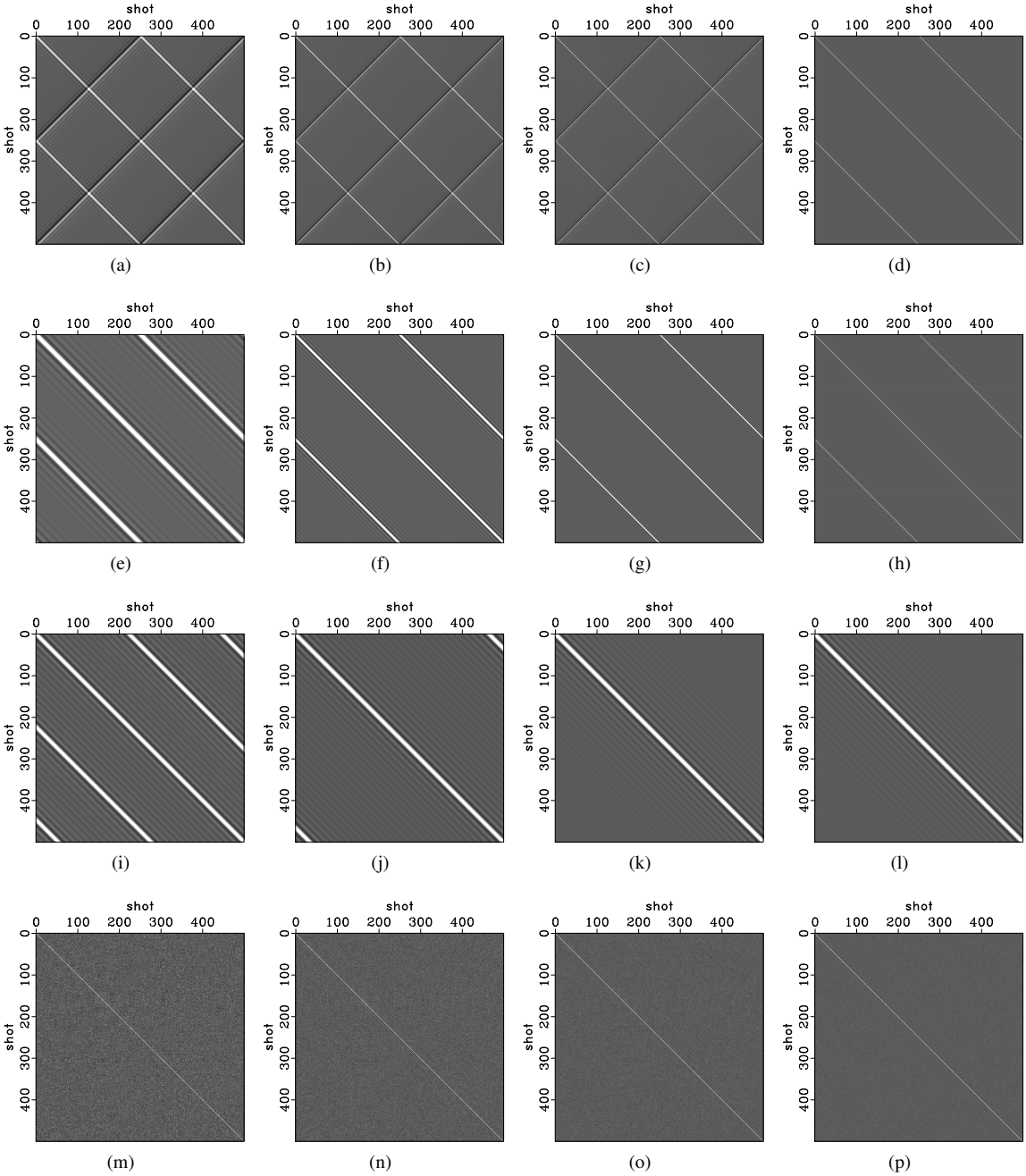


Figure 3. The real part of the crosstalk matrix for 3.0 Hz for the following shot-encoding schemes (top to bottom): Hartley, DFT , plane-wave and random-phase. Each column represents a different number of encodings used with the same shot-encoding scheme from (left to right): 25, 50, 100, 250. All of the crosstalk matrices except those for random-phase encoding have zero imaginary component, which we do not show here for brevity.

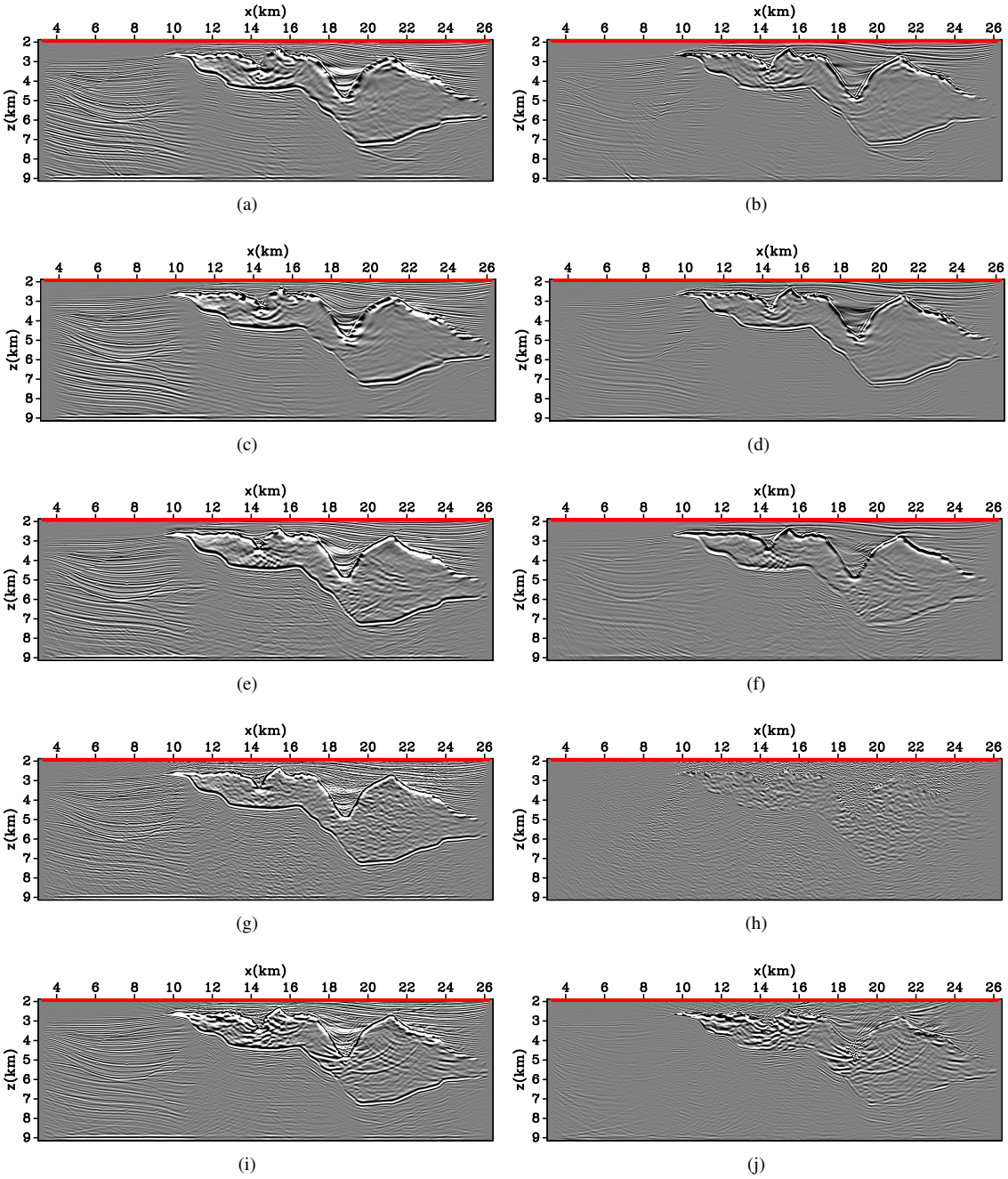


Figure 4. The stacked images (left) and difference images (right) for the following shot-encoding schemes (from top-bottom): Hartley, DFT (modulated-shot), plane-wave, random phase, and decimated shot-record migration. All encodings shown here use 25 encodings.

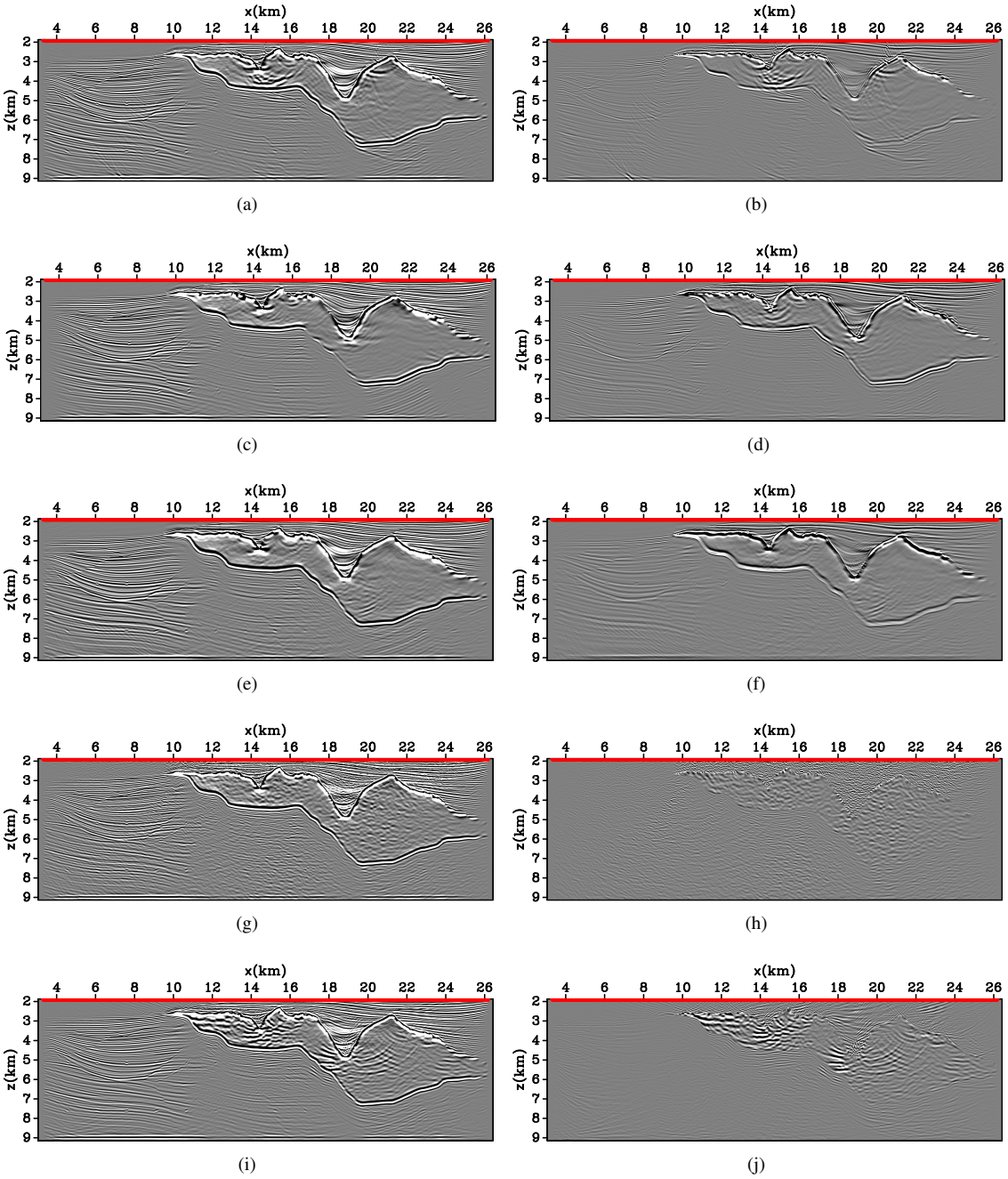


Figure 5. The stacked images (left) and difference images (right) for the following shot-encoding schemes (from top-bottom): Hartley, DFT (modulated-shot), plane-wave, random phase, and decimated shot-record migration. All encodings shown here use 50 encodings.

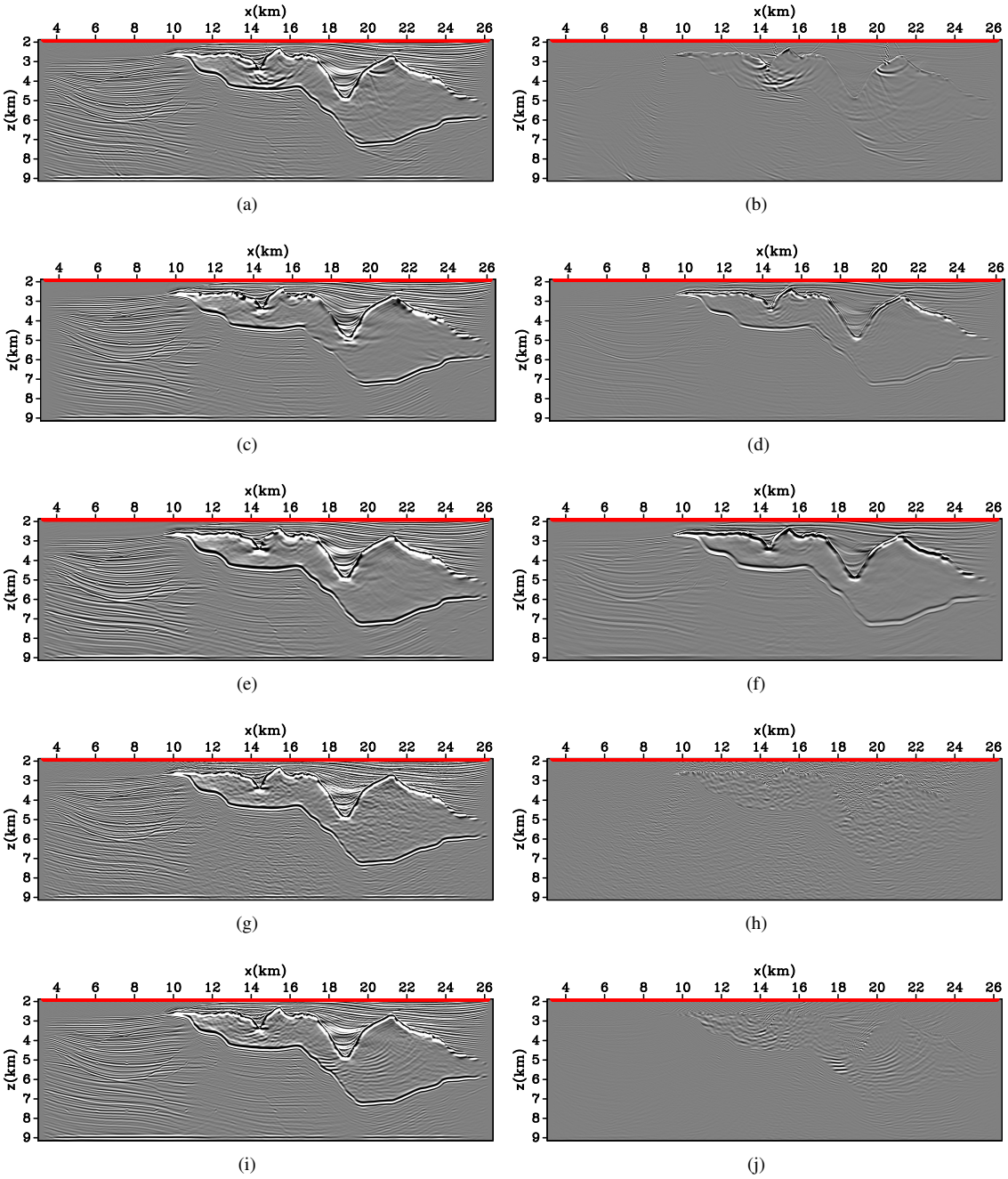


Figure 6. The stacked images (left) and difference images (right) for the following shot-encoding schemes (from top-bottom): Hartley, DFT (modulated-shot), plane-wave, random phase, and decimated shot-record migration. All encodings shown here use 100 encodings.

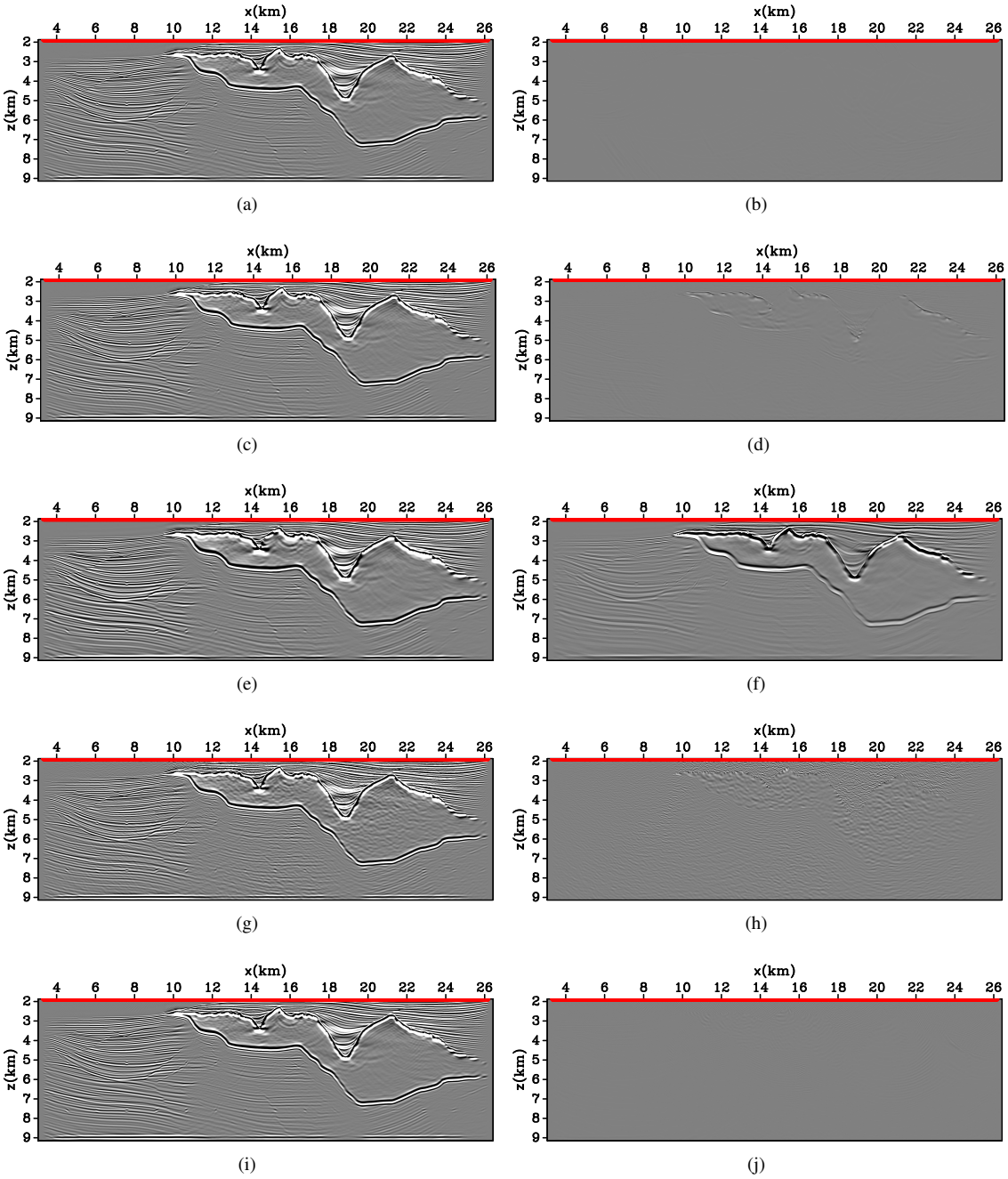


Figure 7. The stacked images (left) and difference images (right) for the following shot-encoding schemes (from top-bottom): Hartley, DFT (modulated-shot), plane-wave, random phase, and decimated shot-record migration. All encodings shown here use 250 encodings.

Shot-encoding scheme	Hartley	DFT	Plane-wave	Random-time	DSRM
Frequency dependent	N	N	Y	Y	N
Migration aperture L_e	$2L_s$	$2L_s$	$2L_s$	$2L_s$	L_s
Γ - 25 experiments	10-20	10-20	10-20	10-20	20
Γ - 50 experiments	5-10	5-10	5-10	5-10	10
Γ - 100 experiments	2.5-5	2.5-5	2.5-5	2.5-5	5
Γ - 250 experiments	1-2.5	1-2.5	1-2.5	1-2.5	2.5

Table 1. Table comparing the computational cost of various shot-encoding schemes with the cost of conventional SRM for all 500 shot-records. The ratio Γ indicates the cost-advantage of blending over SRM. When Γ is greater than one, then blending is more efficient than SRM by that amount (e.g. $\Gamma = 2$ means the encoding is twice as efficient). We show Γ as a range from the worst-case scenario, migrating over a larger aperture significantly increases the computational cost, to the best-case scenario, where there is no increase in cost from migrating over a larger aperture.

crosstalk matrix. Since these shots add together, the amplitudes of the reflectors are distorted overall. This effect is most pronounced for plane-wave migration.

As Figures 4-7 show, the quality of the stacked image for blended imaging greatly depends on the choice of shot-encoding scheme and the number of encodings that we use for imaging. For most shot-encoding schemes the quality of the image increases as the number of encodings increases, which is not a surprising finding. However, the best comparison of the shot-encoding schemes is to measure the energy in the difference images between the blended image and the conventional image, Figure 8. This comparison shows that the best shot-encoding scheme varies with the number of encodings. For example, when using 25 encodings, random-time encoding produces the best quality image, whereas for 100 shot-encodings the best shot-encoding scheme is the Hartley amplitude encoding. We note that random-phase encoding only gradually improves compared to Hartley encoding which improves faster in a fewer number of encodings. Plane-wave migration shows that as the number of encodings increases the overall value for the energy in the difference image relative to conventional SRM is basically the same. One possible explanation is that plane-wave migration is efficient at reconstructing the image as quickly as possible (i.e. using a few encodings), and so the subsequent encodings do not add much information to the image. Overall though, plane-wave migration produces a good quality image, because the artifacts introduced by it are weakly coherent and partially stack out when stacking over frequencies.

However, decimated shot-record migration seemingly produces the best quality image at the lowest computational cost, even with the artifacts caused by spatial aliasing. When we take into account the effect of the larger migration aperture on the cost of blended imaging, then decimated shot-record migration is even more attractive than blended imaging because in the "worst-case" scenario (for blended imaging) decimated shot-record migration is twice as efficient as blending for Sigsbee (i.e. we should compare the results for blending for 25 experiments to the results for decimated shot-record migration using 50 experiments). This result is somewhat surprising, because decimated shot-record migration is not directly equivalent to blended imaging. In particular, there is more information contained in the blended image than in the decimated image, because we use all of the shots from the survey. The results from decimation though show that a good majority of this information is simply redundant and discarded during the blending process.

It does not appear at that an "optimal" shot-encoding scheme exists. We can state this because all shot-encodings are in essence a truncated orthogonal basis. Since there is no known truncated orthogonal basis that allows us to construct a crosstalk matrix that is the identity matrix, we have to use a shot-encoding that always degrades the image in some way. However, there is still a possibility that a shot-encoding exists that produces an image with minimal image degradation compared to already known shot-encoding schemes, but we leave this task for further research as it is a difficult combinatorial problem.

9 CONCLUSIONS

We develop a new class of shot-encoding schemes which modify the amplitudes of the shot-records prior to migration. We compare the results of the Hartley amplitude encoding with existing shot-encoding schemes including: modulated-shot migration, plane-wave migration, and random time-delay encoding. Additionally, we compare those shot-encodings with decimated shot record migration. As expected the various shot-encodings produce images that have different crosstalk characteristics. We find that no one shot-encoding scheme excels over all the others in all circumstances. Instead, we find that the different shot-encodings have different strengths and weaknesses. However, the best images at the lowest possible computational cost are obtained with decimated shot-record migration even in the presence of aliasing artifacts. When we take into account the increased computational cost of migrating blended datasets over larger apertures, the case for decimated shot-record migration instead of blended imaging looks even better.

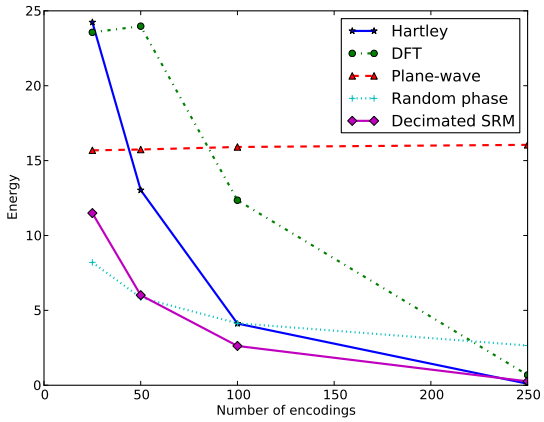


Figure 8. Plots of the energy (lower is better) in the difference image for the various shot-encoding schemes for a group of encodings. The different shot-encodings reconstruct the best quality image at different rates and with different efficiency.

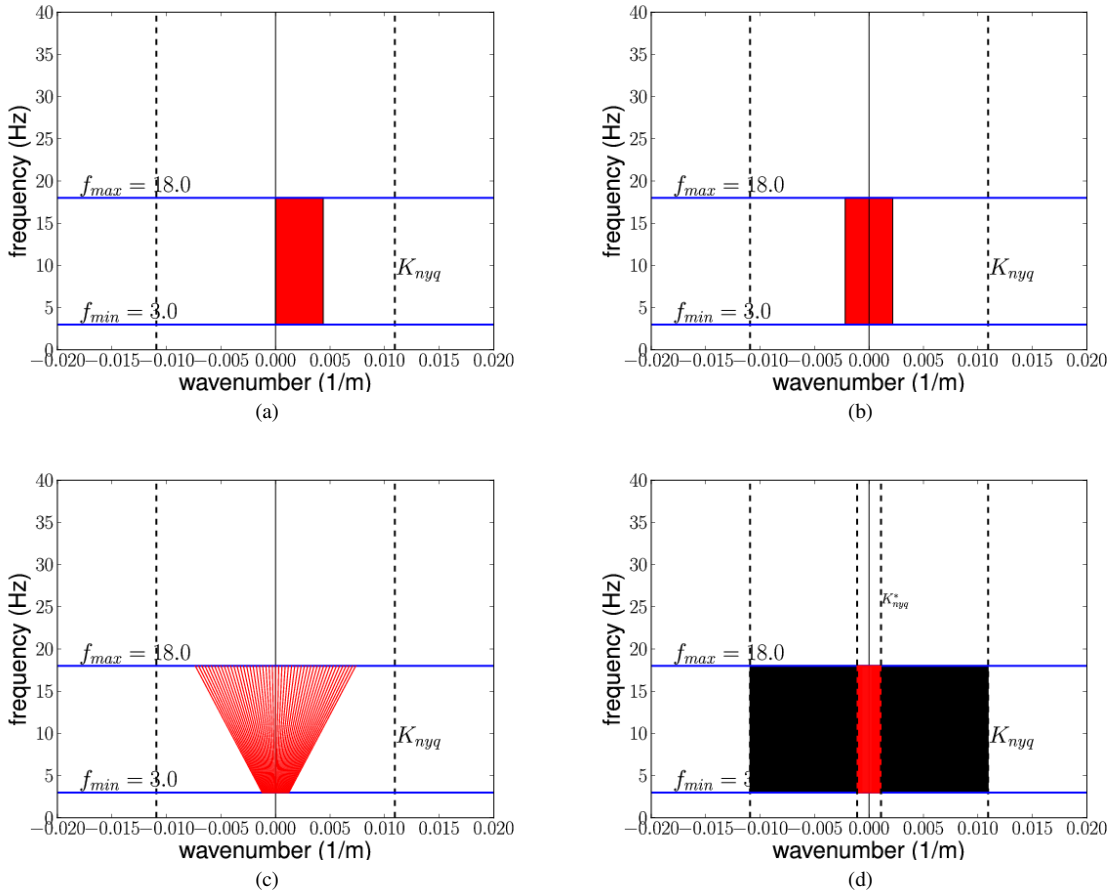


Figure 9. The F-K spectra for the (a) Hartley encoding, (b) DFT encoding, (c) Plane-wave migration, and (d) decimated SRM. All of the spectra show the result of using 50 encodings. f_{min} and f_{max} represent the minimum and maximum frequencies used in the migration, and K_{nyq} represents the Nyquist wave-number. For decimated SRM, K^*_{nyq} represents the new Nyquist wave-number from decimation.

10 ACKNOWLEDGEMENTS

We want to thank the sponsors of the Center for Wave Phenomena for financial support on this project. Also, we want to thank Dave Hale and Francesco Perrone for their insights on various aspects of this project. Lastly, we want to thank the contributors to the Madagascar software package.

REFERENCES

Akerberg, P., G. Hampson, J. Rickett, H. Martin, and J. Cole, 2008, Simultaneous source separation by sparse radon transform: SEG Technical Program Expanded Abstracts, **27**, 2801.

Beasley, C. J., 2008, A new look at marine simultaneous sources: The Leading Edge, **27**, 914.

Berkhout, A., D. Verschuur, and G. Blacquiere, 2009, Seismic imaging with incoherent wavefields: SEG Technical Program Expanded Abstracts, 2894–2898.

Berkhout, A. J. G., G. Blacquiere, and E. Verschuur, 2008, From simultaneous shooting to blended acquisition: SEG Technical Program Expanded Abstracts, **27**, 2831.

Blacquiere, G., G. Berkhout, and E. Verschuur, 2009, Survey design for blended acquisition: SEG Technical Program Expanded Abstracts, 56–60.

Duquet, B., 1999, 3D plane wave migration of streamer data: SEG Technical Program Expanded Abstracts, **20**, 1033.

Hampson, G., J. Stefani, and F. Herkenhoff, 2008, Acquisition using simultaneous sources: The Leading Edge, **27**, 918.

Howard, M., 2007, Marine seismic surveys with enhanced azimuth coverage: Lessons in survey design and acquisition: The Leading Edge, **26**, 480.

Huo, S., Y. Luo, and P. Kelamis, 2009, Simultaneous sources separation via multi-directional vector-median filter: SEG Technical Program Expanded Abstracts, 31–35.

Kapoor, S. J., M. O'Brian, D. Desta, I. Atakishiyev, and M. Tomida, 2007, Subsalt imaging — the RAZ/WAZ experience: SEG Technical Program Expanded Abstracts, **26**, 926.

Kim, Y., I. Gruzinov, M. Guo, and S. Sen, 2009, Source separation of simultaneous source OBC data: SEG Technical Program Expanded Abstracts, 51–55.

Krebs, J. R., J. E. Anderson, D. Hinkley, R. Neelamani, S. Lee, A. Baumstein, and M. Lacasse, 2009, Fast full-wavefield seismic inversion using encoded sources: Geophysics, **74**, WCC177.

Liu, F., 1999, Plane wave source composition: An accurate phase encoding scheme for prestack migration: SEG Technical Program Expanded Abstracts, **21**, 1156.

Liu, F., D. W. Hanson, N. D. Whitmore, R. S. Day, and R. H. Stolt, 2006, Toward a unified analysis for source plane-wave migration: Geophysics, **71**, S129.

Michell, S., E. Shoshitaishvili, D. Chergotis, J. Sharp, and J. Etgen, 2006, Wide azimuth streamer imaging of mad dog; have we solved the subsalt imaging problem?: SEG Technical Program Expanded Abstracts, **25**, 2905.

Moore, I., B. Dragoset, T. Ommundsen, D. Wilson, C. Ward, and D. Eke, 2008, Simultaneous source separation using dithered sources: SEG Technical Program Expanded Abstracts, **27**, 2806.

Morton, S. A., 1999, Fastershot-record depth migrations using phase encoding: SEG Technical Program Expanded Abstracts, **17**, 1131.

Oppenheim, A., 1999, Discrete-time signal processing, 2nd ed. ed.: Prentice Hall.

Perrone, F., and P. Sava, 2009, Comparison of shot encoding functions for reverse-time migration: SEG Technical Program Expanded Abstracts, 2980–2984.

Rietveld, W. E. A., 1994, Prestack depth migration by means of controlled illumination: Geophysics, **59**, 801.

Romero, L. A., D. C. Ghiglia, C. C. Ober, and S. A. Morton, 2000, Phase encoding of shot records in prestack migration: Geophysics, **65**, 426.

Shan, G., and B. Biondi, 2008, Plane-wave migration in tilted coordinates: Geophysics, **73**, S185.

Shoshitaishvili, E., K. Lee, S. Michell, and J. Etgen, 2006, Fast wavefield migration for wide azimuth data.: , 2524–2528.

Soubaras, R., 2006, Modulated-shot migration: SEG Technical Program Expanded Abstracts, **25**, 2430.

Spitz, S., G. Hampson, and A. Pica, 2008, Simultaneous source separation: A prediction-subtraction approach: SEG Technical Program Expanded Abstracts, **27**, 2811.

Stoffa, P. L., M. K. Sen, R. K. Seifoullaev, R. C. Pestana, and J. T. Fokkema, 2006, Plane-wave depth migration: Geophysics, **71**, S261.

Stork, C., 1999, How many p values do you want to migrate for delayed shot wave equation migration?: SEG Technical Program Expanded Abstracts, **23**, 1041.

Strang, G., 1997, Wavelets and filter banks, rev. ed. ed.: Wellesley-Cambridge Press.

Sun, P., 1999, Prestack migration of areal shot records with phase encoding: SEG Technical Program Expanded Abstracts, **21**, 1172.

Temme, P., 1984, A comparison of common-midpoint, single-shot, and plane-wave depth migration: Geophysics, **49**, 1896.

Tieman, H. J., 1997, Improving plane-wave decomposition and migration: Geophysics, **62**, 195.

Ting, C., and W. Zhao, 2009, A simulated wide azimuth simultaneous shooting experiment: SEG Technical Program Expanded Abstracts, 76–80.

Tsitsas, N. L., 2010, On block matrices associated with discrete trigonometric transforms and arising in wave propagation theory: Journal of Computational Mathematics.

Womack, J. E., 1990, Encoding techniques for multiple source point seismic data acquisition: Geophysics, **55**, 1389.

Zhang, Y., J. Sun, and S. Gray, 2007, Reverse-time migration: Amplitude and implementation issues: SEG Technical Program Expanded Abstracts, **26**, 2145.

Zhang, Y., J. Sun, C. Notfors, S. H. Gray, L. Chernis, and J. Young, 2005, Delayed-shot 3D depth migration: Geophysics, **70**, E21.